

opment, London, 1976); C. P. Duncan, S. G. Schladow, W. G. Williams, *Int. Hydrogr. Rev.* **59**, 67 (1982); A. L. Gordon, *J. Geophys. Res.* **72**, 6207 (1967); C. J. Grant and J. R. Wyatt, *Bull. Mar. Sci.* **30**, 613 (1980); M. M. Ibarra, *An. Inst. Biol. Univ. Nac. Auton. Mex. Ser. Cienc. Mar. Limnol.* **13**, 31 (1986); T. N. Lee et al., *Cont. Shelf Res.* **12**, 971 (1992); T. N. Lee, M. E. Clarke, E. Williams, A. F. Szmant, T. Berger, *Bull. Mar. Sci.* **54**, 621 (1994); H. A. Lessios, *Annu. Rev. Ecol. Syst.* **19**, 371 (1988); F. E. Muller-Karger, C. R. McClain, T. R. Fisher, W. E. Esaias, R. Varela, *Prog. Oceanogr.* **23**, 23 (1989); F. E. Muller-Karger and R. Varela, *Mem. Soc. Cien. Natur. la Salle.* **49–50**, 361 (1990); F. E. Muller-Karger and R. Aparicio Castro, *Cont. Shelf Res.* **14**, 199 (1994); H. H. Roberts, P. A. Wilson, A. Lugo-Fernández, *ibid.* **12**, 809 (1992); W. J. Schmitz Jr., J. R. Luyten, R. W. Schmitt, *Bull. Mar. Sci.* **53**, 1048 (1993); W. J. Sturges, C. Evans, S. Welsh, W. Holland, *J. Phys. Oceanogr.* **23**, 250 (1993); V. M. V. Vidal, F. V. Vidal, J. M. Pérez-Molero, *J. Geophys. Res.* **97**, 2155 (1992); V. M. V. Vidal, F. V. Vidal, A. F. Hernández, E. Meza, J. M. Pérez-Molero, *ibid.* **99**, 7571 (1994); R. A. Watlington and M. Concepcion Donoso, in *International Oceanographic Commission's International Workshop on Oceanography in Relation to Sustainable Development and Related Coastal Area Management* (IOC, UNESCO, Paris, 1994).

3. With passive dispersal, the distance a larva can travel primarily depends on current strength and the duration of the larval period. J. W. McManus and L. A. B. Meñez [Abstracts, *8th International Coral Reef Symposium, Panama 1996* (Smithsonian Tropical Research Institute, Balboa, Panama, in press)] have compiled data on dispersal periods for 188 species of coral reef fish. The median larval dispersal period was approximately 1 month, and around 85% of species had dispersal durations of less than 2 months.
4. J. B. C. Jackson, *Coral Reefs* **16** (suppl.), 523 (1997).
5. Z. Sary, thesis, University of the West Indies, Barbados (1995).
6. C. M. Roberts, *Trends Ecol. Evol.* **12**, 35 (1997).
7. ———, *Conserv. Biol.* **9**, 815 (1995).
8. ——— and N. V. C. Polunin, *Rev. Fish Biol. Fish.* **1**, 65 (1991).
9. J. W. McManus, *Ambio* **23**, 181 (1994).
10. J. M. Leis, *Bull. Mar. Sci.* **53**, 362 (1993).
11. D. R. Robertson, *Coral Reefs* **15**, 132 (1996).
12. I. C. Stobutzki and D. R. Bellwood, *J. Exp. Mar. Biol. Ecol.* **175**, 275 (1994).
13. ———, *Mar. Ecol. Prog. Ser.* **149**, 35 (1997).
14. G. P. Jones and M. Milicich, Abstracts, *8th International Coral Reef Symposium, Panama 1996* (Smithsonian Tropical Research Institute, Balboa, Panama, in press).
15. P. J. Doherty, S. Planes, P. Mather, *Ecology* **76**, 2373 (1995).
16. Interaction distances among reefs at each of the 18 sites were measured along north, south, east, and west axes. In addition, maximum and minimum interaction distances were measured for each transport envelope. The average minimum and maximum interaction distances ($n = 18$) were 53 and 448 km (1 month) and 79 and 780 km (2 months) for supply, and 58 and 702 km (1 month) and 89 and 996 km (2 months) for delivery.
17. R. A. Menzies and J. M. Kerrigan, *Proc. Gulf Caribb. Fish. Inst.* **31**, 164 (1979).
18. J. M. Lacson, *Mar. Biol.* **112**, 327 (1992).
19. J. R. Gold, L. R. Richardson, C. Furman, T. L. King, *ibid.* **116**, 175 (1993).
20. J. G. Hateley and T. D. Sleeter, *Bull. Mar. Sci.* **52**, 993 (1993).
21. A. G. Johnson, W. A. Fable Jr., C. B. Grimes, L. Trent, J. Vasconcelos Perez, *Fish. Bull. U.S.* **92**, 91 (1993).
22. M. J. Shulman and E. Bermingham, *Evolution* **49**, 897 (1995).
23. S. J. Katz, C. B. Grimes, K. W. Able, *Fish. Bull. U.S.* **81**, 41 (1983).
24. D. E. Campton, C. J. Berg Jr., L. M. Robinson, R. A. Glazer, *ibid.* **90**, 250 (1992).
25. J. M. Lacson and D. C. Morizot, *Mar. Biol.* **110**, 353 (1991).
26. Supported by the U.S. Agency for International Development's Research Grants Program for Historically Black Universities and Colleges. I greatly appreciate the freedom that L. Ragster and F. Mills of the Eastern Caribbean Center of the University of the Virgin Islands gave me to pursue the initial stages of this work. J. Hawkins provided an excellent sounding board for my ideas from germination to fruition and helped to

prepare the manuscript. J. Leis provided helpful comments on connectivity. I also thank J. Ogden and T. Agardy for inviting me to present this research at the annual meeting of the Society for Conservation Biology in Victoria in 1997.

29 July 1997; accepted 8 October 1997

Crystal Structure of Methyl-Coenzyme M Reductase: The Key Enzyme of Biological Methane Formation

Ulrich Ermler,* Wolfgang Grabarse, Seigo Shima, Marcel Goubeaud, Rudolf K. Thauer

Methyl-coenzyme M reductase (MCR), the enzyme responsible for the microbial formation of methane, is a 300-kilodalton protein organized as a hexamer in an $\alpha_2\beta_2\gamma_2$ arrangement. The crystal structure of the enzyme from *Methanobacterium thermoautotrophicum*, determined at 1.45 angstrom resolution for the inactive enzyme state $MCR_{ox1-silent}$, reveals that two molecules of the nickel porphinoic coenzyme F_{430} are embedded between the subunits α , α' , β , and γ and α' , α , β' , and γ' , forming two identical active sites. Each site is accessible for the substrate methyl-coenzyme M through a narrow channel locked after binding of the second substrate coenzyme B. Together with a second structurally characterized enzyme state (MCR_{silent}) containing the heterodisulfide of coenzymes M and B, a reaction mechanism is proposed that uses a radical intermediate and a nickel organic compound.

Methyl-coenzyme M reductase is the key enzyme of methane formation in methanogenic Archaea. It catalyzes the reduction of methyl-coenzyme M (methyl-CoM) [$CH_3-S-CoM$, 2-(methylthio)ethanesulfonate] with coenzyme B (CoB) (CoB-S-H, 7-thioheptanoyl-threoninephosphate) to methane and the heterodisulfide of CoM (CoM-S-H, 2-thioethane sulfonate) and CoB under strictly anaerobic conditions (1, 2).

About 10^9 tons of CH_4 are produced per year by the reaction in Scheme 1. Part of it escapes to the atmosphere and acts as a potent greenhouse gas (3). Methyl-CoM reductase was first characterized by Ellefson and Wolfe (4) as a yellow protein of an apparent molecular mass of 300 kD composed of three different subunits arranged in an $\alpha_2\beta_2\gamma_2$ configuration. The hexameric protein contains two molecules of the tightly but not covalently bound coenzyme F_{430} (4), which is a Ni porphinoic (5).

Spectroscopic investigations of methyl-

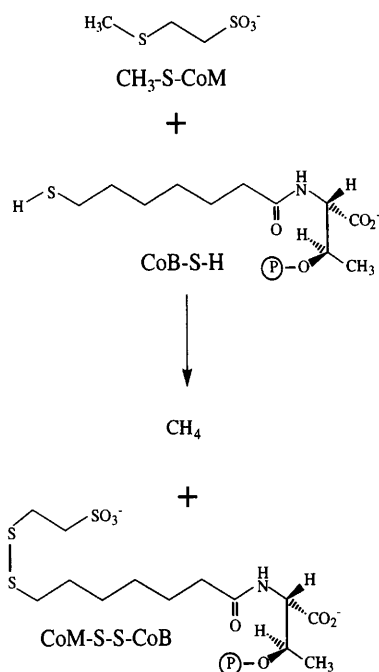
CoM reductase have revealed several Ni electron paramagnetic resonance (EPR) active and inactive states of the enzyme (6). After harvest of H_2-CO_2 grown cells, the enzyme is present in an inactive EPR silent state designated as MCR_{silent} . In this state, methyl-CoM reductase contains bound CoM (7) and CoB (8) and can only be partially reactivated by enzymatic reduction (9). When cells are gassed with H_2 before harvesting, the enzyme is present in an active MCR_{red1} state whose characteristic Ni(I) F_{430} EPR spectrum, designated red 1, can be correlated with the enzymatic activity in the enzyme (10). Even under strictly anaerobic conditions, the activity of the enzyme is completely lost within a few hours, and the enzyme enters an inactive EPR-silent Ni(II) state denoted as $MCR_{red1-silent}$. When cells are gassed with CO_2-N_2 before being harvested, the enzyme enters into the MCR_{ox1} state, which exhibits a Ni EPR spectrum, designated ox1, substantially different from that of the MCR_{red1} state. The MCR_{ox1} state has only very low activity but can be activated in vitro by reduction with Ti(III) citrate (11) into the MCR_{red1} state. Preparations in the MCR_{ox1} state slowly turn into an inactive EPR silent state, referred to as $MCR_{ox1-silent}$.

Methyl-CoM reductase (isoenzyme I) was aerobically crystallized in the enzymatically inactive enzyme states $MCR_{ox1-silent}$ and MCR_{silent} , as described by Shima et al.

U. Ermler, Max-Planck-Institut für Biophysik, Heinrich-Hoffmann-Straße 7, 60528 Frankfurt, Germany. W. Grabarse, Max-Planck-Institut für Biophysik, Heinrich-Hoffmann-Straße 7, 60528 Frankfurt, Germany, and Max-Planck-Institut für Terrestrische Mikrobiologie und Laboratorium für Mikrobiologie der Philipps-Universität, Karl-von-Frisch-Straße, 35043 Marburg, Germany. S. Shima, M. Goubeaud, R. K. Thauer, Max-Planck-Institut für Terrestrische Mikrobiologie und Laboratorium für Mikrobiologie der Philipps-Universität, Karl-von-Frisch-Straße, 35043 Marburg, Germany.

*To whom correspondence should be addressed.

(12). The crystal structure was solved in the $MCR_{ox1-silent}$ state at 2.9 Å resolution by the method of multiple isomorphous replacement (Table 1) and refined to current R_{cryst} and R_{free} values (Table 1) of 19.5 and 22.0%, respectively, in the resolution range 1.45 to 10.0 Å. The structure of the MCR_{silent} state was refined to current R_{cryst} and R_{free} values of 18.0 and 22.4%, respectively, in the resolution



Scheme 1

Fig. 1. Structure of methyl-CoM reductase. Ribbon diagram of the heterohexamer. Secondary structure segments were defined according to DSSP (40). Subunits α and α' are depicted in red and orange, subunits β and β' in dark green and light green, and subunits γ and γ' in dark blue and light blue. Subunit α can be subdivided into an NH_2 -terminal region ($\alpha 3$ to $\alpha 101$), an $\alpha + \beta$ domain ($\alpha 102$ to $\alpha 276$), an α helix domain ($\alpha 277$ to $\alpha 506$), and a $COOH$ -terminal region ($\alpha 506$ to $\alpha 549$). The $\alpha + \beta$ domain consists of a four-stranded antiparallel β sheet flanked by extended helical regions. This fold is reminiscent of the α, β sandwich motif of the $\beta\alpha\beta\beta\alpha\beta$ class (41) found, for example, in a formyltransferase (42), which is another protein of the methanogenic pathway. The α -helix domain of subunit α is composed of eight α helices of variable length, building up a helix sandwich structure in a way similar (43) to that observed for the transmembrane domain of diphtheria toxin (44). The general architecture of subunit β and the fold of the $\alpha + \beta$ domain and the α -helix domain resemble those of subunit α , suggesting a common ancestor. Subunit γ is primarily built up by an α, β sandwich folding unit ($\gamma 81$ to $\gamma 160$) that corresponds again to the subclass of doubly intertwined $\beta\alpha\beta\beta\alpha\beta$ folding motifs. As observed for subunits α and β , subunit γ has also extended NH_2 -terminal ($\gamma 2$ to $\gamma 80$) and $COOH$ -terminal ($\gamma 202$ to $\gamma 248$) regions serving as contact arms to other subunits. The positions of the coenzymes F_{430} (displayed in yellow) indicate the approximate location of the two active sites. Figures 1 and 4 were produced with MOLSCRIPT (45) and RASTER3D (46).

range 2.0 to 10.0 Å with the use of the $MCR_{ox1-silent}$ structure for initial phase determination. The model of the $MCR_{ox1-silent}$ state is mainly distinguished from that of MCR_{silent} by binding of CoM and CoB in the reduced form instead of the oxidized heterodisulfide form of CoM and CoB. The two enzyme states exhibit a nearly identical overall structure. In both structures, the electron density map reveals five modified amino acids located in subunits α and α' at or very near the active site region. The observed 1-*N*-methyl-His $^{\alpha 257}$, 4-methyl-Arg $^{\alpha 271}$, 2-methyl-Gln $^{\alpha 400}$, and *S*-methyl-Cys $^{\alpha 452}$, as well as Gly $^{\alpha 445}$, where the carbonyl oxygen appears to be substituted by sulfur, have to be confirmed by biochemical analysis.

The overall structure of methyl-CoM reductase is characterized by a series of α helices arranged in a compact form with an ellipsoidal shape (Fig. 1) of about 120 by 85 by 80 Å. The subunits are mutually tightly associated, as indicated by extended interface areas, particularly between subunits α and α' and subunits β and β' , and by the fact that, except for subunits γ and γ' , each subunit contacts all other subunits of the multisubunit complex (Fig. 1). The fold of the subunits is described in the legend of Fig. 1.

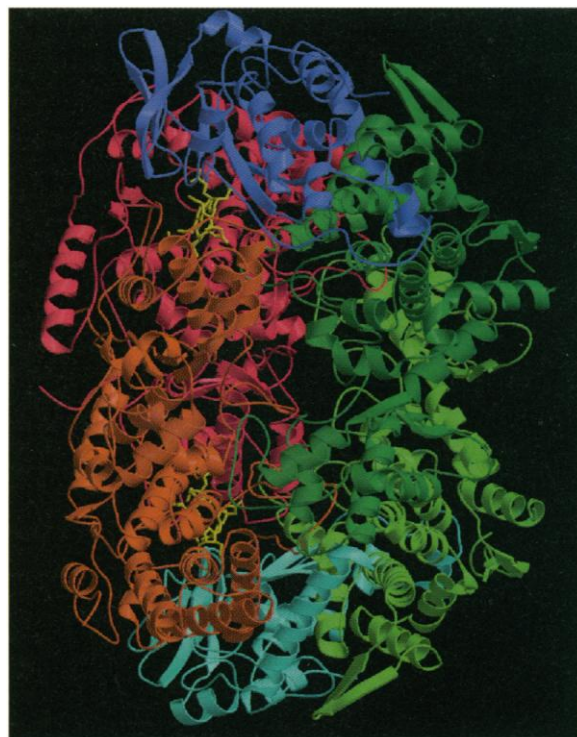
The binding sites of two sets of coenzymes F_{430} , M, and B are roughly 50 Å apart (Fig. 1), forming two separated structurally identical active sites. The $MCR_{ox1-silent}$ and MCR_{silent} structures reveal that coenzymes F_{430} , M, and B and the heterodisulfide CoM-S-S-CoB, respectively, are embedded inside a narrow channel, 30 Å long, extend-

ing from the protein surface deeply into the interior of the protein complex (Fig. 2, A and B). The channel and the coenzyme binding sites are formed by residues of subunits α , α' , β , and γ (and equivalently α' , α , β' , and γ'), indicating that one trimer is not sufficient to accomplish the enzymatic reaction. The overall structure looks as if the protein has been developed from an $\alpha_2\beta_2$ tetramer with vestigial channels at the appropriate interfaces.

Coenzyme F_{430} fits neatly into a pocket at the apex of the channel inside the protein (13). Its tetrapyrrole plane is oriented such that its front face (reduced pyrrole rings A, B, C, and D clockwise, Fig. 3) points roughly toward the mouth of the channel, whereas its rear face points to the channel apex.

Because of the excellent quality of the electron density map (Fig. 3), the structure of coenzyme F_{430} could be confirmed, particularly the absolute configuration of the pyrrole substituents derived previously by nuclear magnetic resonance, circular dichroism, and x-ray studies (5). The tetrapyrrole ring of coenzyme F_{430} is bound in a rather flat conformation to the enzyme, as predicted for the free coenzyme F_{430} in the hexagonally coordinated Ni(II) state (5).

When analyzing the noncovalent interactions between the Ni porphyrinoid and the polypeptide chain, two features are particularly striking. First, the five negative charges of the deeply buried F_{430} carboxylate groups are neutralized by ionic interactions only to a minor extent, but they are delocalized by a



series of hydrogen bonds. The presence of the carboxylate groups in the charged state is likely because of their exclusive contacts with hydrogen donors. Second, coenzyme F_{430} not only has a large number of interactions, but it is also apparently rigidly bound

to the protein. Fifteen of the 21 hydrogen bonds between coenzyme and protein are formed to peptide amide nitrogens.

Table 1. X-ray structure determination. Crystals of methyl-CoM reductase from *M. thermoautotrophicum* grown with 25% polyethylene glycol 400 as precipitant have the space group $P2_1$ and unit cell dimensions of $a = 83.1 \text{ \AA}$, $b = 120.2 \text{ \AA}$, $c = 123.1 \text{ \AA}$, and $\beta = 91.70^\circ$ with one hexamer per asymmetric unit (12). Native data (Nat1, Nat2, and Nat3) and eight heavy-atom derivative data sets [Hg1, thimerosal; Hg2, mersalylic acid; Hg3, $C_2H_5HgPO_4$; Hg4, CH_3HgCl ; Pt1, K_2PtCl_4 ; Pt2, di- μ -iodobis(ethylenediamine)-di-platinum nitrate; Pt3, $K_2PtCl_2(NH_2)_2$; and Au, $KAuCl_4$] were collected with a Rigaku rotating anode x-ray generator producing CuK_α radiation and an image plate detector (Mar-Research, Hamburg, Germany). Reflections were processed with MOSFLM (30), DENZO (31), and the CCP4 program suite (32). The Patterson map of Hg1 was interpreted with SHELXS (33). Heavy-atom positions were refined and phases were computed with MLPHARE (34). Phases were improved by solvent flattening with DM (35) and molecular averaging with RAVE (36). The quality of the resulting electron density maps to a resolution of 2.9 \AA was sufficient to incorporate nearly the complete polypeptide model with the known primary structure (37). Model building was done within the program O (38). The coordinates were refined by means of the simulated annealing and positional refinement protocol of X-PLOR (39) with data set Nat2 collected at the Max-Planck beam line at the Deutsches Elektronensynchrotron (Hamburg) for the $MCR_{ox1-silent}$ state and data set Nat3 measured in house for the MCR_{silent} state. After refinement, the root-mean-square deviation from ideal stereochemical parameters is 0.009 \AA for bond lengths and 1.30° for bond angles. The average temperature factor is 9 \AA^2 . The model of the $MCR_{ox1-silent}$ state comprises residues $\alpha 3$ to $\alpha 549$, $\beta 2$ to $\beta 443$, $\gamma 2$ to $\gamma 248$, $\alpha' 3$ to $\alpha' 549$, $\beta' 2$ to $\beta' 443$, and $\gamma' 2$ to $\gamma' 248$; two sets of coenzymes F_{430} , B, and M; one Zn^{2+} molecule; two Mg^{2+} molecules; and 1320 water molecules.

Data sets	Nat1	Nat2	Nat3	Hg1	Hg2	Hg3	Hg4	Pt1	Pt2	Pt3	Au
Resolution (\AA)	2.9	1.45	2.0	2.9	4.3	3.1	3.5	3.1	2.9	4.7	4.9
Completeness (%)	91	96	92	93	94	85	84	84	83	82	88
Multiplicity	2.1	4.3	3.4	2.2	2.2	1.8	2.2	2.5	2.2	2.0	2.4
R_{sym} (%) [*]	5.6	6.6	8.1	5.1	5.2	7.1	8.0	5.9	5.2	5.4	3.4
R_{der} (%) [†]				14.0	13.8	13.7	18.8	14.3	17.9	14.6	9.5
Phasing power [‡]				1.5	1.6	1.6	1.7	1.5	1.4	1.4	1.3
R_{Cullis} (%) [§]				0.53	0.61	0.54	0.66	0.60	0.62	0.54	0.71

^{*} $R_{sym} = \sum_{hkl} \sum_i |I_i - \langle I \rangle| / \sum_i I_i$, where I_i is the intensity of the i th measurement per reflection hkl and $\langle I \rangle$ is the average intensity for a reflection hkl . [†] $R_{der} = \sum_{hkl} |F_{P1} - |F_{P1}|| / \sum_{hkl} |F_{P1}|$, where $|F_{P1}|$ and $|F_{P1}|$ are the structure factor amplitudes for the native protein and the heavy-atom derivatives, respectively. [‡]Phasing power is defined as F_H/E , where F_H is the calculated heavy-atom structure factor and $E[\sum_{hkl} (|F_{PH} - F_P|) - F_H]$ is the residual lack of closure. [§] $R_{Cullis} = E[\sum_{hkl} (|F_{PH} - F_P|)]$; it is related to centric reflections. $R_{Cyst. free} = \sum |F_{obs} - |F_{calc}|| / \sum |F_{obs}|$, where F_{obs} and F_{calc} are the observed and calculated structure factors, respectively. The free reflections (5% of the total) were held aside throughout the refinement.

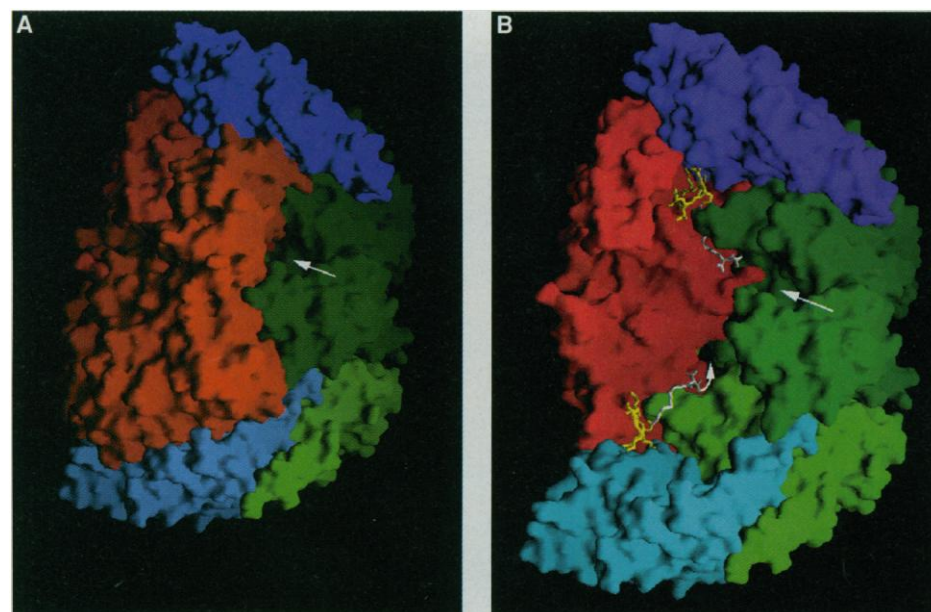


Fig. 2. (A) Molecular surface representation of methyl-CoM reductase that shows the entrance of one of the channels (indicated by a white arrow). The two channels are formed by subunits α , α' , β , and γ and α' , α , β' , and γ' , respectively. The colors of the subunits are as in Fig. 1. (B) Molecular surface of methyl-CoM reductase without subunit α' allows a view into the interior of the channels, showing the binding place of the coenzymes. Coenzymes F_{430} are yellow, and the heterodisulfides of coenzymes M and B are white. The entrances of both channels are indicated by a white arrow. This figure was generated with GRASP (47).

The Ni atom present as Ni(II) sits almost exactly in the tetrapyrrole plane and is coordinated to six ligands arranged in a nearly optimal octahedral configuration (Fig. 4, A and B). The four equatorially located nitrogen atoms of the tetrapyrrole ring have distances to the nickel of 2.14 \AA for ring A, 2.11 \AA for ring B, 2.10 \AA for ring C, and 1.99 \AA for ring D, compared with 2.09 \AA as derived from x-ray absorption spectroscopic studies (14). As the fifth ligand, the side chain oxygen of $Gln^{\alpha 147}$ protrudes from a long loop between helix 5 and strand D of the $\alpha + \beta$ domain to the rear face of F_{430} and approaches the Ni atom to 2.3 \AA . The 1.45 \AA electron density map demonstrates that the oxygen and not the nitrogen of the side chain of $Gln^{\alpha 147}$ is the axial ligand. The sixth coordination site of nickel located in front of the tetrapyrrole ring plane of F_{430} is occupied by the thiol group of CoM in the $MCR_{ox1-silent}$ structure and by a sulfonate oxygen of the heterodisulfide in the MCR_{silent} structure (Fig. 4, A and B). The distance between nickel and sulfur is 2.4 \AA ; between nickel and oxygen, it is 2.1 \AA .

The analysis of the $MCR_{ox1-silent}$ structure reveals that CoM is positioned almost parallel to the tetrapyrrole plane in contact with its front face (Fig. 4A). The thiol

to the protein. Fifteen of the 21 hydrogen bonds between coenzyme and protein are formed to peptide amide nitrogens.

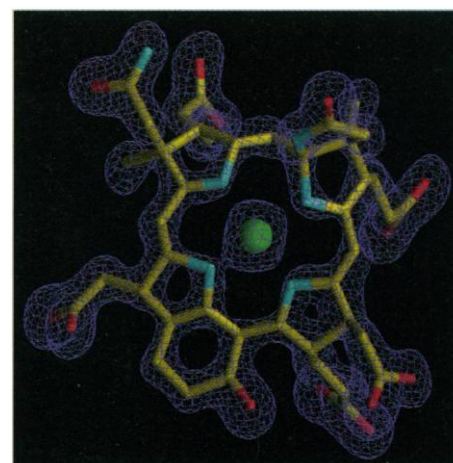


Fig. 3. Structure of coenzyme F_{430} (viewed toward the front face) and the final $2|F_{obs}| - |F_{calc}|$ electron density at 1.45 \AA resolution contoured at the 2σ level. The quality of the electron density is sufficiently high to determine the exact configuration of the coenzyme that is in agreement with previous results (5). The propionate substituents of rings A, B, and C are perpendicular to the tetrapyrrole plane pointing toward the apex, whereas the lactam ring is directed toward the mouth of the channel (Fig. 2B). The six-membered carbocyclic ring joined with ring D, and the protruding acetate and acetamide substituents lie approximately in the tetrapyrrole ring plane. Figures 3 and 5 were produced with SETOR (48).

group binds axially to the nickel and interacts with the hydroxyl groups of Tyr^{α333} and Tyr^{β367} and a water molecule that bridges CoM and CoB. The ethyl moiety is embedded between the lactam ring of the Ni porphyrinoid and the phenyl ring of Phe^{α443}. Coenzyme M is anchored to the polypeptide chain by its negatively charged sulfonate group, forming a salt bridge to the guanidinium group of Arg^{γ120}, a hydrogen bond to the peptide nitrogen of Tyr^{α444}, and a hydrogen bond to a water molecule connected to the peptide oxygen of His^{β364} (Fig. 4A).

With its elongated conformation, CoB fits accurately into the most narrow segment of the channel formed by residues of subunits α, α', and β (Fig. 2). Coenzyme B is anchored to the protein mainly by salt bridges between the negatively charged threoninephosphate moiety and five positively charged amino acids (Fig. 5). The heptanoyl arm is in van der Waals contact with several hydrophobic residues. The thiol group of CoB interacts with the side chain nitrogen of Asn^{α481}, the main chain peptide nitrogen of Val^{α482}, and the bridging water molecule mentioned above (Fig. 5). Asn^{α481} is within hydrogen bond distance of the sulfur that is presumed to replace the backbone carbonyl oxygen of the modified Gly^{α445}. A functional role of this modification is therefore possible.

Although CoM and CoB bind separately in the MCR_{ox1-silent} state (Fig. 4A), they are covalently linked as a heterodisulfide in the MCR_{silent} state (Fig. 4B). A superposition of

the structures reveals that the reduced CoB and the CoB moiety of the heterodisulfide align perfectly except that the sulfur is turned slightly toward CoM. In contrast to CoB, CoM has moved more than 4 Å away from its position in the MCR_{ox1-silent} state. The thiol group is shifted perpendicular and the sulfonate group parallel to the tetrapyrrole plane of F₄₃₀, resulting in a 90° rotation of CoM. In this position, one oxygen atom of the sulfonate is axially coordinated with the nickel and contacts the hydroxyl group of Tyr^{α333}. The second oxygen atom is hy-

drogen-bonded to the lactam ring of F₄₃₀ and to the hydroxyl group of Tyr^{β367} and the third to a water molecules located at the former binding site of the sulfonate (Fig. 4B).

Both the MCR_{ox1-silent} and the MCR_{silent} structures display inactive states of methyl-CoM reductase with coenzyme F₄₃₀ bound in the Ni(II) oxidation state. Nevertheless, the arrangement of the coenzymes and their protein environment, combined with the available biochemical and spectroscopical data, allow for conclu-

Fig. 5. The CoB binding in the MCR_{ox1-silent} structure. Coenzyme B binds in an elongated conformation into the most narrow segment of the channel built up of residues of subunits α (red), α' (orange), and β (green). The enzymatically relevant thiol group is directed to the apex, whereas the threoninephosphate moiety points toward the mouth of the channel. Only the phosphate and the carboxylate groups are accessible to bulk solvent. The threoninephosphate moiety is strongly linked to the protein mainly by salt bridges between both the phosphate and carboxylate group and five basic amino acid residues. Arg^{α270}, His^{β379}, Lys^{α'256}, and methyl-His^{α'257} interact with the phosphate group and Arg^{α'225} and Lys^{α'256} with the carboxylate group. Arg^{α271} neighboring Arg^{α270} is methylated.

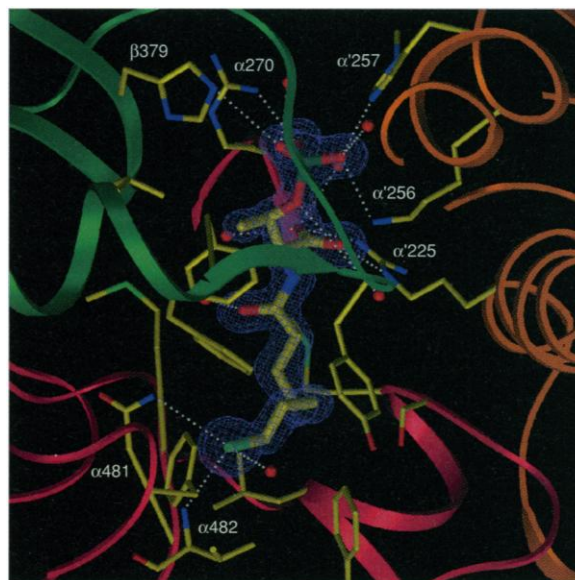
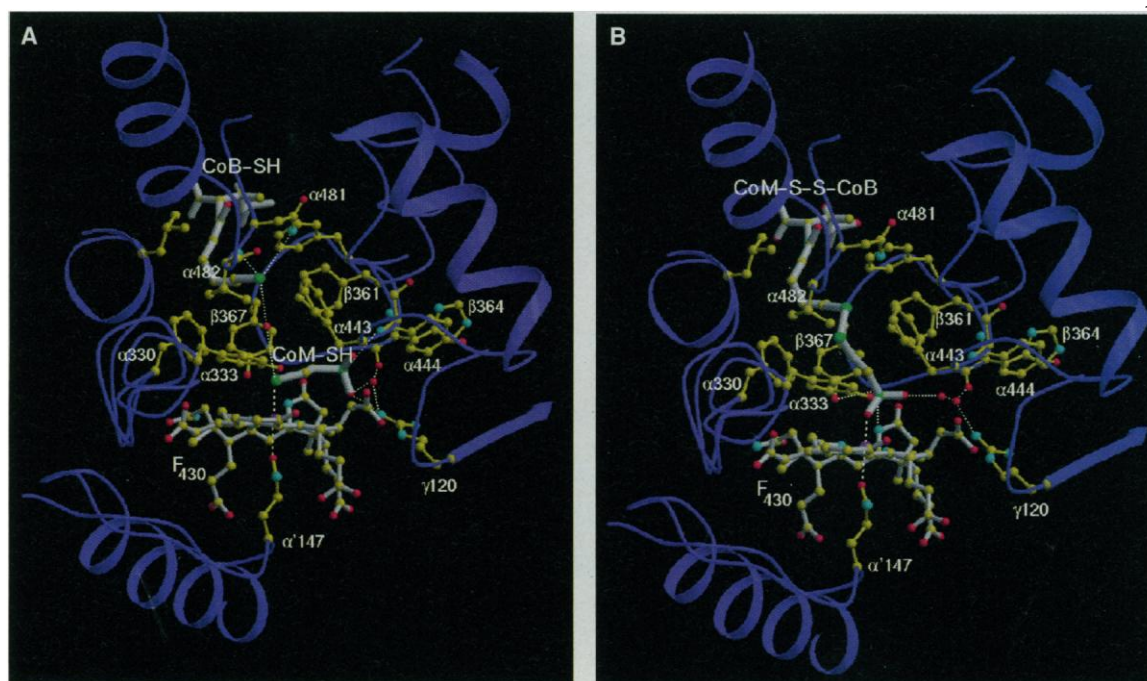


Fig. 4. (A) The active site region of the MCR_{ox1-silent} structure. The binding positions of the coenzymes suggest the active site between the nickel of coenzyme F₄₃₀ and the sulfur atom of CoB. The active site is coated mostly by non-polar and aromatic residues. Five mutually contacting phenylalanine and tyrosine side chains are arranged as ring forming a tunnel. (B) The active site region of the MCR_{silent} structure. Compared with the MCR_{ox1-silent} structure, CoM has moved through the tunnel to form with CoB a heterodisulfide, the oxidation product of the reaction. The sulfonate moiety of CoM lost its interactions to the protein matrix and is coordinated to the Ni atom.



sions about the active site and a proposal for the catalytic mechanism outlined in Fig. 6.

First of all, the two structurally identical active sites separated from each other by roughly 50 Å (Fig. 1) appear to exclude all mechanisms requiring two molecules of coenzyme F_{430} in methane formation from methyl-CoM and CoB.

The relative arrangement of the three coenzymes (Fig. 4) suggests that the catalytic reaction takes place at the front side of coenzyme F_{430} in the channel between the nickel and the thiol groups of CoB (Figs. 2 and 4). Each active site is lined up by an annular arrangement of Phe $^{\alpha 330}$, Tyr $^{\alpha 333}$, Phe $^{\alpha 443}$, Phe $^{\beta 361}$, and Tyr $^{\beta 367}$ flanked by further hydrophobic and aromatic residues (Fig. 4). These amino acids are completely conserved in all methyl-CoM reductases (15). The active site region is accessible only through one channel and only for small molecules up to a diameter of 6 Å (16). This channel is completely locked when CoB is bound (17), shielding the

active site from bulk solvent (Figs. 2 and 5). The sole water molecule found in the active site region of $MCR_{ox1-silent}$ between CoM and CoB should be displaced after the binding of the more bulky methyl-CoM. Methane formation from methyl-CoM and CoB thus takes place in a hydrophobic aromatic environment and probably does not involve water molecules. These conditions would allow for radical intermediates, which have been proposed (18–20) and accounted for in the proposed reaction mechanism outlined in Fig. 6. Solvent-inaccessible active sites coated by nonpolar aromatic residues and attainable by a channel have also been observed in several radical-based enzymes, such as galactose oxidase (21), prostaglandin- H_2 synthase-1 (22), and methylmalonyl-coenzyme A mutase (23).

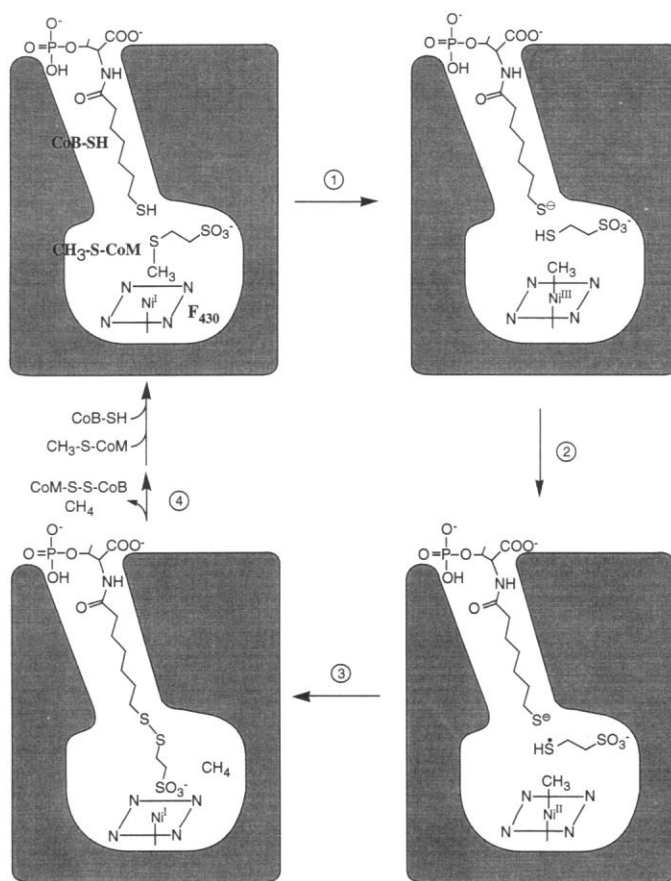
During the catalytic reaction of methane formation, CoB releases and the activated methyl group accepts a hydrogen atom. The $MCR_{ox1-silent}$ structure reveals an interaction between the thiol group of CoB and two hydrogen donors, the amide and pep-

ptide nitrogens of Asn $^{\alpha 481}$ and Val $^{\alpha 482}$ (Fig. 5), which would facilitate the cleavage of a proton and permit the presence of a thiolate anion (Fig. 6). However, the CoB sulfur is 6 Å from the tentatively modeled Ni-CH $_3$, which is probably too far away for direct hydrogen transfer. Therefore, the participation of CoM as hydrogen mediator between CoB and the activated methyl group (Fig. 6), perhaps through Tyr $^{\alpha 333}$ or Tyr $^{\beta 367}$ (Fig. 4), is an attractive possibility. The distances of their phenolate oxygens to the nickel are 4.4 and 4.3 Å and to the modeled methyl group are around 3.1 and 3.3 Å, respectively.

In the $MCR_{ox1-silent}$ structure (Fig. 4A), CoM probably mimics the binding position of methyl-CoM with respect to the binding mode of the sulfonate moiety but presumably not with respect to the binding mode of the thiol group. A Ni-S-CoM intermediate in the catalytic cycle is not attractive because of the large distance of 6.2 Å between the sulfurs of CoM and CoB. Model building studies indicate, however, that the two sulfurs of CoM and CoB come in van der Waals contact when the methyl group of methyl-CoM is placed in van der Waals distance of the potentially attacking nickel. Therefore, a Ni-CH $_3$ intermediate proposed from free coenzyme F_{430} studies (19, 24, 25) appears to be compatible with the steric requirements of the active site (see Fig. 6). The proximity of the sulfurs of CoM and CoB in the model allows for heterodisulfide formation that could induce a shift of CoM toward CoB and thus loosen the interactions between the sulfonate moiety of CoM and the protein matrix.

In the structure of MCR_{silent} (Fig. 4B), the bound heterodisulfide CoM-S-S-CoB cannot leave the enzyme because a sulfonate oxygen of CoM binds to the Ni(II) atom of F_{430} . However, both protein and coenzyme conformations might be very close to an intermediate of the enzymatic reaction after product formation (Fig. 6, lower left), assuming that a coordination of the sulfonate oxygen to nickel is prevented when, under reducing conditions, nickel is present as nucleophilic Ni(I). The repulsion between Ni(I) and the sulfonate oxygen molecules might even be used as a driving force to push the heterodisulfide out of the channel. It is not evident at present where and how the methane gets out.

Fig. 6. Cartoon 1 showing the proposed steps in methane formation from methyl-CoM and CoB. The reaction cycle starts (step 1) with a nucleophilic attack of Ni(I) on the methyl group of CoM, forming a methyl-Ni(III) organic compound. Model reactions indicate that the methyl transfer reaction is facilitated when the leaving group is protonated (19). Perhaps the proton originates from CoB. In step 2, the strongly oxidative Ni(III) (19) withdraws an electron from the protonated CoM, generating a CoM thiol radical that is a strong acid and therefore dissociates. In step 3, the methyl-Ni(II) generated in step 2 is protonolyzed in a spontaneous reaction (19, 49). Almost simultaneously, the CoM thiol radical couples with the thiolate group of CoB, and the surplus electron of the generated disulfide anion radical is returned to Ni(II). In step 4, methane and CoM-S-S-CoB are released, and the next cycle can be started after renewed binding of methyl-CoM and CoB. The two Ni(I) intermediates (lower and upper left of the figure) are related to the MCR_{red1} state of the enzyme described in the text. The MCR_{silent} state is probably derived from the MCR_{red1} state (lower left) by one electron oxidation. The MCR_{ox1} state could be formed by reaction of the CoM thiol radical with Ni(II) after protonolysis of the methyl-Ni(II) intermediate, yielding a Ni(III) thiolate adduct. $MCR_{ox1-silent}$ would then be derived from MCR_{ox1} by one electron reduction.



REFERENCES AND NOTES

1. R. S. Wolfe, *Annu. Rev. Microbiol.* **45**, 1 (1991).
2. R. K. Thauer, *Antonie Leeuwenhoek* **71**, 21 (1997).
3. K. B. Hogan, J. S. Hoffman, A. M. Thompson, *Nature* **354**, 181 (1991).
4. W. L. Ellefson and R. S. Wolfe, *J. Biol. Chem.* **256**, 4259 (1981).
5. A. Pfaltz *et al.*, *Helv. Chim. Acta* **65**, 828 (1982); G. Färber *et al.*, *ibid.* **74**, 697 (1991).

6. S. P. J. Albracht *et al.*, *Biochim. Biophys. Acta* **955**, 86 (1988).
7. P. L. Hartzell, M. J. Donnelly, R. S. Wolfe, *J. Biol. Chem.* **262**, 5581 (1987).
8. K. M. Noll and R. S. Wolfe, *Biochem. Biophys. Res. Commun.* **139**, 889 (1986).
9. P. E. Rouvière and R. S. Wolfe, *J. Bacteriol.* **171**, 4556 (1989).
10. S. Rospert, R. Böcher, S. P. J. Albracht, R. K. Thauer, *FEBS Lett.* **291**, 371 (1991).
11. M. Goubeaud, G. Schreiner, R. K. Thauer, *Eur. J. Biochem.* **243**, 110 (1997).
12. S. Shima, M. Goubeaud, D. Vinzenz, R. K. Thauer, U. Ermler, *J. Biochem.* **121**, 829 (1997).
13. The small diameter of the channel prevents the bulky F₄₃₀ from entering methyl-CoM reductase in the hexameric state and suggests an association to one of the subunits before oligomerization (26).
14. R. A. Scott, P. L. Hartzell, R. S. Wolfe, J. LeGall, S. P. Cramer, in *Frontiers of Bioinorganic Chemistry*, A. V. Xavier, Ed. (VCH, New York, 1986), pp. 20–26.
15. J. Nolling *et al.*, *Int. J. Syst. Bacteriol.* **46**, 1170 (1996).
16. Methyl-CoM must therefore enter the channel before CoB to attain its binding site, which is consistent with the ordered ternary complex kinetic mechanism displayed by the enzyme (27).
17. Coenzyme B was found to be unable to penetrate the 30 Å long channel far enough so that its thiol group at the end of a long aliphatic arm can reach the Ni atom of coenzyme F₄₃₀ at the apex of the channel. The distance of 8.7 Å between the sulfur and the Ni atoms makes a Ni-S-CoB intermediate in the catalytic cycle, as has been proposed (18), unlikely. In this respect, it is of interest that CoB homologs with a (CH₂)₅ or (CH₂)₇ rather than a (CH₂)₆ aliphatic arm were shown to be inhibitory (28).
18. A. Berkessel, *Bioorg. Chem.* **19**, 101 (1991).
19. B. Jaun, in *Metal Ions in Biological Systems*, H. Siegel and A. Siegel, Eds. (Dekker, New York, 1993), vol. 29, pp. 287–337.
20. ———, *Helv. Chim. Acta* **73**, 2209 (1990).
21. N. Ito *et al.*, *Nature* **350**, 87 (1991).
22. D. Picot, P. J. Loll, R. M. Garavito, *ibid.* **367**, 243 (1994).
23. F. Mancía *et al.*, *Structure* **4**, 339 (1996).
24. S.-K. Lin and B. Jaun, *Helv. Chim. Acta* **74**, 1725 (1991).
25. ———, *ibid.* **75**, 1478 (1992).
26. P. L. Hartzell and R. S. Wolfe, *Proc. Natl. Acad. Sci. U.S.A.* **83**, 6726 (1986).
27. L. G. Bonacker, S. Baudner, E. Mörschel, R. Böcher, R. K. Thauer, *Eur. J. Biochem.* **217**, 587 (1993).
28. J. Ellermann, R. Hedderich, R. Böcher, R. K. Thauer, *ibid.* **172**, 669 (1988).
29. Y. Ahn, J. A. Krzycki, H. G. Floss, *J. Am. Chem. Soc.* **113**, 4700 (1991).
30. A. G. W. Leslie, *ESF/CCP4 Newsl. Protein Crystallogr.* **26**, 83 (1992).
31. Z. Otwinowski, in *Data Collection and Processing*, L. Sawyer, N. Issacs, S. Bailey, Eds. (Daresbury Laboratory, Warrington, UK, 1993), pp. 56–62.
32. Collaborative Computational Project, Number 4, *Acta Crystallogr. D* **50**, 760 (1994).
33. G. H. Sheldrick, in *Proceedings of the CCP4 Study Weekend*, W. Wolf, P. R. Evans, A. G. W. Leslie, Eds. (Daresbury Laboratory, Warrington, UK, 1991), pp. 23–38.
34. Z. Otwinowski, in *ibid.*, pp. 80–86.
35. K. D. Cowtan, *ESF/CCP4 Newsl. Protein Crystallogr.* **31**, 83 (1994).
36. G. A. Kleywegt and T. A. Jones, in *Proceedings of the CCP4 Study Weekend*, S. Bailey, R. Hubbard, D. Waller, Eds. (Daresbury Laboratory, Warrington, UK, 1994), pp. 59–66.
37. M. Bokranz, G. Bäumner, R. Allmansberger, D. Ankel-Fuchs, A. Klein, *J. Bacteriol.* **170**, 568 (1988).
38. T. A. Jones, J. Y. Zou, S. W. Cowan, M. Kjeldgaard, *Acta Crystallogr. A* **47**, 110 (1991).
39. A. T. Brünger, *X-PLOR Manual, Version 3.1*. (Yale University, New Haven, CT, 1992).
40. W. Kabsch and C. Sander, *Biopolymers* **22**, 2577 (1983).
41. C. A. Orengo and J. M. Thornton, *Structure* **1**, 105 (1993).
42. U. Ermler, M. C. Merckel, R. K. Thauer, S. Shima, *ibid.* **5**, 635 (1997).
43. L. Holm and C. Sander, *J. Mol. Biol.* **233**, 123 (1993).
44. S. Choe *et al.*, *Nature* **357**, 216 (1992).
45. P. J. Kraulis, *J. Appl. Crystallogr.* **24**, 946 (1991).
46. E. A. Merrif and M. E. P. Murphy, *Acta Crystallogr. D* **50**, 869 (1994).
47. A. Nicholls, R. Bharadwaj, B. Honig, *Biophys. J.* **64**, 166 (1993).
48. S. V. Evans, *J. Mol. Graphics* **11**, 134 (1993).
49. One could hypothesize an alternative reaction mechanism involving a transient methyl radical intermediate, which might account for the presumed methylation of His²⁵⁷, Arg²⁷¹, Gln⁴⁰⁰, and Cys⁴⁵². Such a mechanism is not excluded by the finding that methyl-CoM reduction to methane mainly proceeds with inversion of the stereo configuration (29).
50. We thank D. Vinzenz for crystallization, H. Michel for generous support and for reading the manuscript, K. Diederichs for reading the manuscript, C. Kratky for providing us with coordinates of coenzyme F₄₃₀ analogs, B. Jaun for discussions, and the staff of the Max-Planck beamline at the Deutsches Elektronensynchrotron Hamburg for help during data collection. The cartoon in Fig. 6 was suggested by R. Cammack (King's College, London). The coordinates of the MCR_{ox1-silent} structure will be deposited in the Protein Data Bank with the accession number 1mro.

15 August 1997; accepted 6 October 1997

Targeting of HIV- and SIV-Infected Cells by CD4-Chemokine Receptor Pseudotypes

Michael J. Endres,* Salman Jaffer, Beth Haggarty, Julie D. Turner, Benjamin J. Doranz, Peter J. O'Brien, Dennis L. Kolson, James A. Hoxie

Retroviral vectors containing CD4 and an appropriate chemokine receptor were evaluated for the ability to transduce cells infected with human immunodeficiency virus (HIV) and simian immunodeficiency virus (SIV). These CD4-chemokine receptor pseudotypes were able to target HIV- and SIV-infected cell lines and monocyte-derived macrophages in a manner that corresponded to the specificity of the viral envelope glycoprotein for its CD4-chemokine receptor complex. This approach could offer a way to deliver antiviral genes directly to HIV-infected cells *in vivo* and could provide an additional treatment strategy in conjunction with existing antiviral therapies.

Treatment of HIV-infected patients with combinations of antiretroviral drugs has resulted in a profound reduction of detectable virus in plasma and lymph tissue and is expected to have considerable clinical benefit (1). However, recent studies of subpopulations of resting T cells from peripheral blood and lymph nodes have shown that reservoirs of HIV-infected cells persist in most patients despite several months of therapy (2). New strategies to target HIV-infected cells could provide important adjunctive approaches to therapy. Recently, rhabdoviruses containing CD4 and the chemokine receptor CXCR4 were shown to superinfect HIV-infected cell lines, presumably by interacting with viral envelope glycoproteins on the cell surface (3). The demonstration that viral receptors can be used to target HIV-infected cells represents an approach with potentially broad clinical and pharmacologic applications (4). We now

demonstrate that retroviral vectors pseudotyped with CD4 and different chemokine receptors are also able to transduce HIV- and SIV-infected cells in a manner that reflects the receptor specificity of the viral envelope glycoprotein. In addition, we show that this approach can be used to target HIV-infected macrophages as well as cell lines.

Entry of HIV and SIV is mediated by interactions between the viral envelope glycoprotein and a cellular receptor complex, which consists of CD4 and one or more members of the CC or CXC chemokine receptor family of proteins (5). The specificity of this interaction largely determines the tropism of the virus for particular cell types. Thus, macrophage tropic (M-tropic) HIV isolates as well as most SIV isolates require CCR5, T cell line-tropic (T-tropic) isolates (for example, IIIB) require CXCR4, and dual tropic HIV isolates (for example, 89.6) are able to use both CXCR4 and CCR5. Other recently described chemokine receptors can also function with CD4 as coreceptors for HIV and SIV (6).

To create retroviral particles coated with functional HIV or SIV receptor complexes, we cotransfected QT6 quail cells with plasmids encoding CD4 (pT4-cDNA3), a chemokine receptor (pCXCR4-cDNA3 or pCCR5-cDNA3), and an envelope-deficient HIV-1

M. J. Endres, B. Haggarty, J. D. Turner, P. J. O'Brien, J. A. Hoxie, Department of Medicine, Hematology-Oncology Division, University of Pennsylvania, Philadelphia, PA 19104, USA.
S. Jaffer and D. L. Kolson, Department of Neurology, University of Pennsylvania, Philadelphia, PA 19104, USA.
B. J. Doranz, Department of Pathology and Laboratory Medicine, University of Pennsylvania, Philadelphia, PA 19104, USA.

*To whom correspondence should be addressed. E-mail: endres@mail.med.upenn.edu